Improved techniques for measuring x-ray mass attenuation coefficients

Martin D. de Jonge
Chanh Q. Tran
Christopher T. Chantler
Zwi Barnea
University of Melbourne
Melbourne, Victoria, 3010
Australia
E-mail: dejonge@aps.anl.gov

Abstract. We apply the x-ray extended-range technique (XERT) to measure mass attenuation coefficients over one order of magnitude more accurately than previously reported in the literature. We describe the application of the XERT to the investigation of systematic effects due to harmonic energy components in the x-ray beam, scattering and fluorescence from the absorbing sample, the bandwidth of the x-ray beam, and thickness variations across the absorber. The high-accuracy measurements are used for comparison with different calculations of mass attenuation coefficients, and to identify particular regions where these calculations fail. [DOI: 10.1117/1.2190647]

Subject terms: mass attenuation coefficient; atomic form factor; x-ray extended-range techniques.

Paper 040560R received Aug. 24, 2004; revised manuscript received May 11, 2005; accepted for publication Aug. 17, 2005; published online Apr. 11, 2006. This paper is a revision of a paper presented at the SPIE conference on Optical Constraints of Materials for UV to X-Ray Wavelengths, Aug. 2004, Denver, Colorado. The paper presented there appears (unrefereed) in SPIE Proceedings Vol. 5538.

1 Introduction

The accuracy of x-ray optical constants can significantly affect the optimization of an experimental arrangement and the interpretation of experimental results. For example, x-ray atomic form factors and mass attenuation coefficients can affect the interpretation of tomographic and crystallographic experiments, and can influence the design of x-ray refractive lenses and zone plates. Despite significant differences between various tabulations of mass attenuation coefficients, these tabulations are often used with little discrimination.

Figure 1 presents the percentage difference between the mass attenuation coefficients of molybdenum appearing in the x-ray form factor, attenuation, and scattering tables (FFAST)[1–3] and XCOM[4,5] tabulations. The FFAST values form the zero line. Significant differences between the calculated values are observed across a wide range of energies both above and below the absorption edge of molybdenum at about 20 keV, and exceed 15% at some energies. Similar discrepancies between calculated values are present in all tabulations, for all elements, and across all x-ray energies.

The results of measurements of the mass attenuation coefficients of molybdenum compiled by Hubbell et al.[6,7] are plotted in Fig. 1. These experimental results generally claim uncertainties of between 1 and 2%. The spread of the measurements shows that the measurement accuracy is much poorer than claimed. These measurements are unable to resolve differences between the FFAST and XCOM tabulations. Discrepancies between the results of independent investigations indicate that there are significant and undiagnosed systematic errors that have affected the accuracy of the measurements.[8,9] This work describes our methods for investigating these sources of systematic error and their effects on the measured mass attenuation coefficients.

We use the x-ray extended-range technique (XERT) and

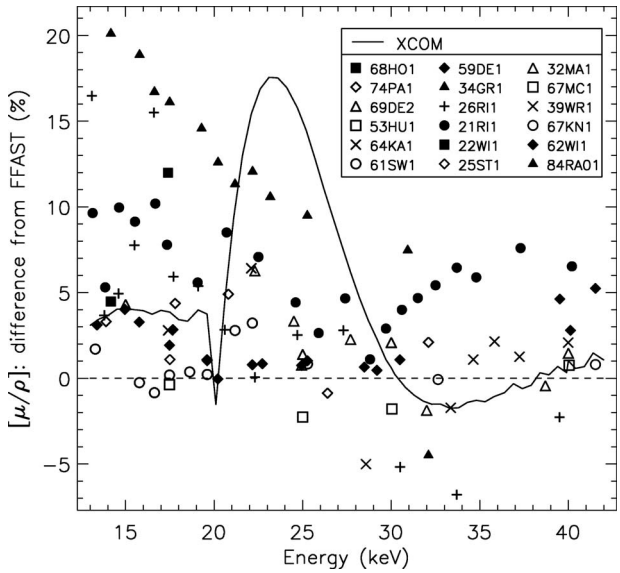

Fig. 1 Discrepancies between theoretical predictions and experimental measurements of the mass attenuation coefficient of molybdenum presented as a percentage difference from the FFAST tabulation.[1–3] The difference between the FFAST and XCOM[4,5] tabulations is greater than about 4% over most of the energy range shown here, but rises to over 15% over several keV above the absorption edge. A variety of measured values are also plotted.[6,7] The experimenter code referred to in the key is as per Hubbell et al.[6,7] Differences of 10 to 20% between measured values whose typical claimed uncertainties are about 2% indicate the presence of unrecognized systematic errors affecting these measurements.

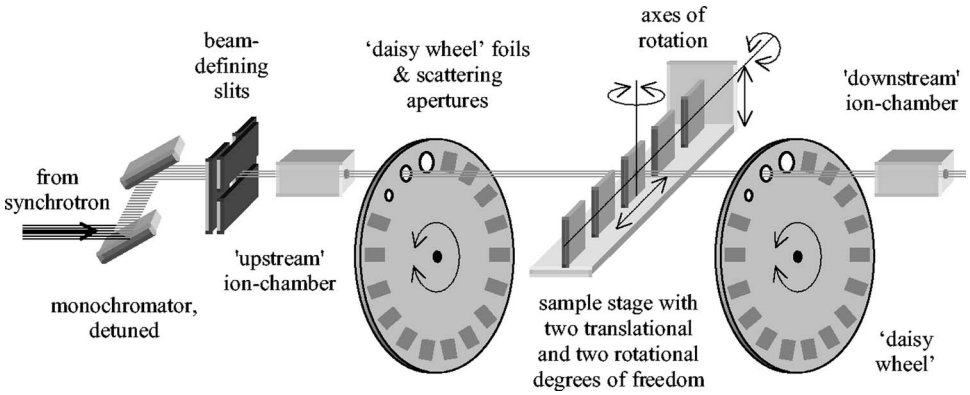

Fig. 2 Typical arrangement of the experimental components used to employ the XERT.

probe a number of dimensions of the measurement parameter space to determine the influence of a range of systematic effects on the measured values.[10] We make measurements under optimum conditions and continue these measurements well beyond the optimum range. Critical examination of the nature of the breakdown of the measurement is used to identify the cause of the measurement failure, and thus to estimate the implications, if any, on measurements made under optimal conditions. In particular, this work describes our treatment of systematic errors arising from the presence of harmonic energy components, the effects of secondary radiation (scattering and fluorescence), the influence of the finite x-ray energy bandwidth, and from absorber thickness variations. These methods have been applied to measurements of the mass attenuation coefficients of copper,[11] silicon,[12] silver,[13] and molybdenum.[14] Explicit tests for the effects of a wide range of systematic errors have enabled us to rigorously justify experimental accuracies of between 0.02 to 0.7%.

Figure 2 presents a schematic of the experimental setup that we have used to measure mass attenuation coefficients. The exact details of the experimental arrangement vary slightly in response to the operational details of the synchrotron beamline. We have used bending magnet, undulator, and elliptical multipole wiggler sources to produce a spectrum of high-brilliance x-rays. The x-ray beam is monochromated by double reflection from a monochromator, usually silicon, and preferably from planes with a "forbidden" second-order reflection [such as (111) or (311)]. The monochromator is usually detuned to reduce the passage of higher-order harmonics into the beam.[15,16]

Counting statistics have limited measurement precision in a number of reported measurements of mass attenuation coefficients.[17–20] We have used high-brilliance synchrotron sources to obtain measurements with high statistical precision. The improved statistical precision of our measurements has made it possible to detect a range of systematic effects that would otherwise not be discernible from the data.

The x-ray beam is collimated to a cross section of approximately 1×1 mm^2 by the use of two orthogonal slits. An upstream ion chamber is used to monitor the intensity of the incident beam, and a downstream ion chamber to record the intensities of the attenuated and unattenuated beams. We use matched ion chambers, and optimize for strong positive correlations between the counts recorded in the upstream and downstream ion chambers.[21,22] Accordingly, gas is flowed through the ion chambers in a serial configuration. We have generally recorded measurements with correlation $R\geqslant0.99$, which enables us to determine the ratio of the measured intensities to high precision. This precision enables us to detect the effects of systematic errors on the measurement with high sensitivity.

A number of specimens of widely differing attenuation ($0.5\leqslant[\mu/\rho][\rho t]\leqslant5$) are used to measure the x-ray attenuation at each energy. The samples are mounted on the sample stage, shown in Fig. 2, which is located midway between the upstream and the downstream ion chambers. The stage can be rotated about two axes and translated in two directions orthogonal to the beam. The samples are placed and replaced in the path of the beam to high precision by the use of a computer-controlled motorized driving system.

Daisy wheels[23] are located between the sample stage and the ion chambers. These daisy wheels have on their perimeters a series of apertures that are used to admit different amounts of secondary (fluorescent and scattered) photons into the ion chambers. In addition to these apertures, a large number of attenuating foils are mounted on the perimeter of the daisy wheels and these can, like the apertures, be placed in the path of the beam by suitable rotation of the daisy wheel. The thicknesses of the daisy-wheel foils are chosen to span an extremely large range of x-ray attenuations, typically with $0.01\leqslant[\mu/\rho][\rho t]\leqslant50$ at the nominal x-ray energy.

2 Harmonic Components

When attenuation measurements are made using a monochromatic x-ray beam, the logarithm of the intensity plotted as a function of the absorber thickness t falls in a straight line whose slope is the product of the mass attenuation coefficient $[\mu/\rho]$ and the density ρ of the foil material, as described by the Beer-Lambert relation

$$\ln\left(\frac{I}{I_0}\right)=-\left[\frac{\mu}{\rho}\right]\rho t, \tag{1}$$

where I and I_0 are the attenuated and unattenuated intensities, respectively. The product $[\mu/\rho]\rho$ is sometimes re-

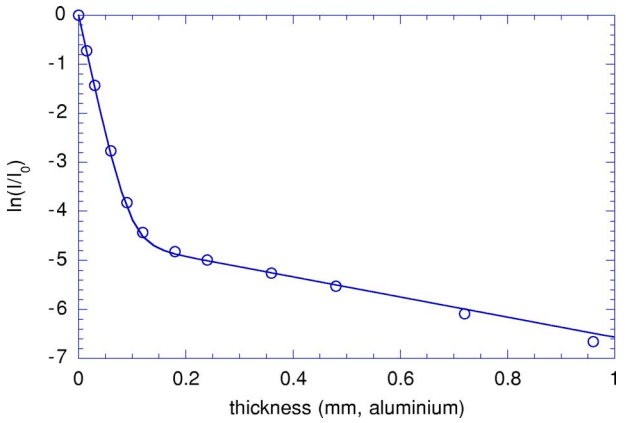

Fig. 3 The attenuation $\ln(I/I_0)$ as a function of the thickness of aluminium absorber in the x-ray beam with a silicon monochromator set to 5 keV. ○ represents experimental values; solid line is the curve of best fit corresponding to an admixture of (1.09±0.02)% third-order harmonic (15 keV) following Eq. (2).

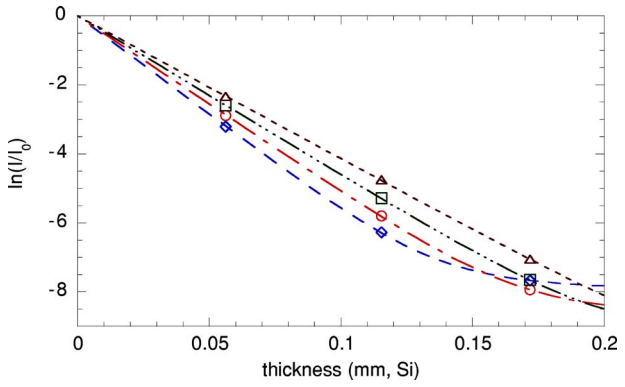

Fig. 4 A harmonic component measurement with three well-calibrated thicknesses provides a constant and reliable indicator of accuracy in attenuation measurements. Measurements were made at: ◇ 5.0 keV, ○ 5.2 keV, □ 5.4 keV, and △ 5.6 keV. Calculated curves for each energy pass through the measured values.

ferred to as the linear absorption coefficient μ, but we use the alternate notation for consistency.

In practice, $\ln(I/I_0)$ can be nonlinear with thickness due to the presence of other spectral components in the beam. In particular, harmonic multiples of the fundamental x-ray energy may be present in the beam, especially when their intensities in the source spectrum are significant. While detuning of the monochromator crystal may suppress the propagation of these harmonic components in the beam, the residual effect on the measured attenuation may nonetheless be significant.

The relative efficiency of detection of the fundamental and of the harmonic x-rays influences the effect of any harmonic components on an attenuation experiment. In particular, the ion-chamber detectors used in our work exhibit a rapid decrease in detection efficiency with increasing x-ray energy, suppressing the harmonic components. However, the *effective* harmonic content, i.e., as perceived by the detector, can still be significant, as was the case in our measurement of the mass attenuation coefficient of silicon,[12] which we describe here.

For a fraction x of harmonic x-rays (with attenuation coefficient $[\mu/\rho]_h$) in the incident monochromatized beam (with $[\mu/\rho]_f$ the attenuation coefficient for the fundamental energy), the measured attenuation of the x-ray beam $[\mu/\rho]_{\text{meas}}\rho t$ will be[23]

$$-\left[\frac{\mu}{\rho}\right]_{\text{meas}}\rho t = \ln\left(\frac{I}{I_0}\right)_{\text{meas}} = \ln\left[(1-x)\exp\left\{-\left[\frac{\mu}{\rho}\right]_f \rho t\right\} + x\exp\left\{-\left[\frac{\mu}{\rho}\right]_h \rho t\right\}\right]. \quad (2)$$

Figure 3 shows the measured attenuation of 11 sets of aluminium foils (with thicknesses between 15 μm and 1 mm) in the path of an x-ray beam monochromated by a detuned, double-reflection silicon (111) channel-cut monochromator set to select 5-keV x-rays. These foils were placed in the beam by suitable rotation of the daisy wheel. This technique is accurate, reproducible, and rapid. This work was performed at the bending magnet beamline 20B of the Photon Factory synchrotron at Tsukuba.

The experimental values follow a straight line until the thickness of aluminium increases to such an extent that the detected radiation consists overwhelmingly of the more energetic 15-keV third-order harmonic. When this occurs, one observes an inflexion with the gradient approaching that of $[\mu/\rho]\rho$ of aluminium at the energy of the third-order harmonic.

This inflexion in the plot provides clear evidence for the presence of a third-order harmonic [the (222) second-order reflection for silicon is forbidden]. The solid curve in Fig. 3 is the calculated thickness dependence of the attenuation of aluminium for 5-keV x-rays with an admixture of (1.09±0.02)% of the 15-keV third-order harmonic, as can be confirmed by extrapolating the second linear portion of the graph back to zero thickness.

A minimum of three samples of accurately known thickness is required to simultaneously determine x, $[\mu/\rho]_f$ and $[\mu/\rho]_h$. If $[\mu/\rho]_h$ is provided by a separate experiment (or theory), then the use of three samples overdetermines the problem and allows for error analysis, or alternatively allows the possible observation of an additional harmonic component. In Fig. 4, we have determined the harmonic content of the beam at several energies by using three well-calibrated thicknesses of silicon. Attenuation measurements of the foils at the harmonic energy, yielding $[\mu/\rho]_h$, have been used to provide the gradient for the harmonic component dominating in the high-thickness portion of the graph. This figure shows clearly the effect of the harmonic components on the mass attenuation coefficient measured using the thickest sample at the lower energies. The harmonic component decreases rapidly as the fundamental energy increases due to the changing ion-chamber efficiencies and the lesser amounts of the harmonic x-rays in the synchrotron source spectrum. Our measurements of the effect of the beam harmonic component have enabled us to determine the mass attenuation coefficient of silicon at these low energies to accuracies of 0.3 to 0.5%.

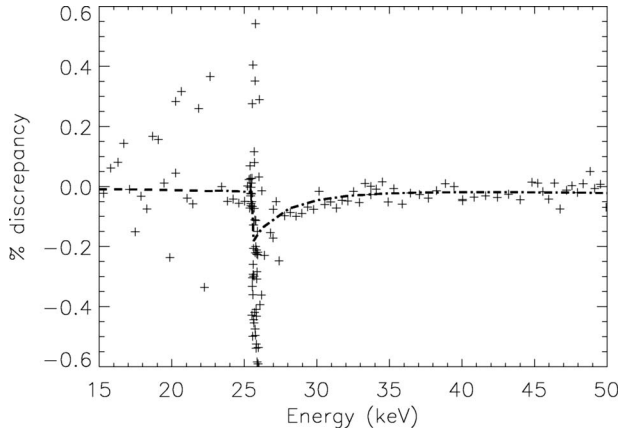

Fig. 5 Percentage discrepancy between the mass attenuation coefficients of silver measured using the large and medium diameter apertures. The dashed and dash-dot lines show the prediction for the 10- and 100-μm foils used for the measurements.

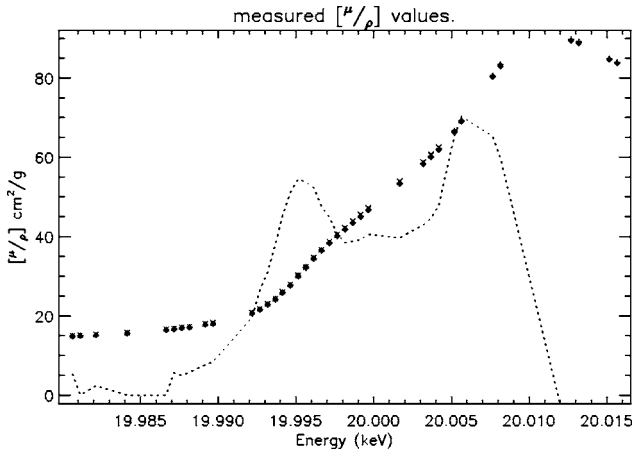

Fig. 6 Values of the mass attenuation coefficient of molybdenum obtained from measurements in the near-edge region. At each energy, measurements have been made with three thicknesses of foil, represented by three different symbols: $\times$ for 100 μm; + for 50 μm; and $\diamond$ for 25 μm. The consistency of the experimental values is too good for the measurements at each energy to be clearly resolved on this scale. The gradient of the weighted mean of the measurements made at each energy is plotted as a dotted line, on a relative scale.

3 Secondary Radiation

The mass attenuation coefficient $[\mu/\rho]$ can be determined accurately using the setup depicted in Fig. 2, provided the ion chambers only record the intensities of the attenuated and unattenuated beams. However, the dominant attenuating processes in the 1- to 100-keV energy range—photoelectric absorption and Rayleigh and Compton scattering—produce secondary x-rays that may also reach the detectors.

Incident x-ray photons may be elastically or inelastically scattered by the absorbing material or by the air path. X-ray fluorescence resulting from photoelectric absorption can contribute significantly to the recorded count rate when measurements are made on the high-energy side of an absorption edge. The contribution of these effects depends on the x-ray optics and collimation, the photon energy, the detector response function, and on the atomic number and thickness of the absorbing sample.

We have made measurements with apertures of various diameters placed between the absorbing specimen and the ion chambers. These apertures, mounted on the daisy wheels, admit various amounts of the secondary radiation into the detectors. The signature of the admission of secondary radiation into the ion chamber is a systematic change in the measured mass attenuation coefficients correlating with the aperture diameter and the sample thickness, and which also varies as a function of photon energy.

Figure 5 shows the percentage discrepancy in the measured mass attenuation coefficients of silver, comparing those obtained with a large (16 mm diam) and medium (8 mm diam) aperture. This figure shows that the value measured using the large aperture is up to 0.2% less than that measured using the medium aperture. This effect is largest immediately above the silver absorption edge at about 25.2 keV, where the fluorescent yield is greatest, and where the incident beam is most attenuated.

We have modeled the effect of the dominant fluorescent and Rayleigh scattered x-rays on the measured mass attenuation coefficients.[24] Our model calculates the contribution to the counts recorded in the upstream and the downstream ion chambers resulting from fluorescent radiation emitted by the absorber and from Rayleigh scattering by the absorbing material and the air path between the ion chambers. Self-absorption corrections are applied to all secondary photons. The prediction of this model is shown in Fig. 5, and is in good agreement with the observed discrepancies. These investigations have been carried out in the course of determining the mass attenuation coefficients of silver accurate to 0.27 to 0.7%.[13]

4 X-Ray Bandwidth

Even the most highly monochromatic source produces a spectrum of x-rays of finite bandwidth. Typical bandwidths vary from $\Delta E/E \approx 10^{-6}$ for characteristic emission lines, to $\Delta E/E \approx 10^{-4}$ for x-rays monochromated by reflection from a crystal monochromator. The most obvious consequence of having a distribution of energies in the x-ray beam is that instead of measuring the mass attenuation coefficient corresponding to a single x-ray energy, we measure the combined attenuation at these energies weighted by the intensity of each x-ray energy component. Since each energy component will in general have a different attenuation coefficient, the original distribution of energies in the x-ray beam—the beam energy profile—will change gradually as the beam is attenuated by the foil, with the less attenuated components gradually increasing their relative intensity over the more attenuated components. This change in the beam energy profile will manifest itself experimentally as a nonlinearity of the measured mass attenuation coefficient as a function of foil thickness.[25]

Away from absorption edges, the mass attenuation coefficient varies sufficiently slowly for the bandwidth effect not to be detected. However, on the absorption edge the mass attenuation coefficient changes rapidly and the effect of the bandwidth is significant. Figure 6 presents the values obtained from measurements made along the molybdenum absorption edge. This work was performed on the 1-ID beamline at X-ray Operations and Research (XOR) sector 1

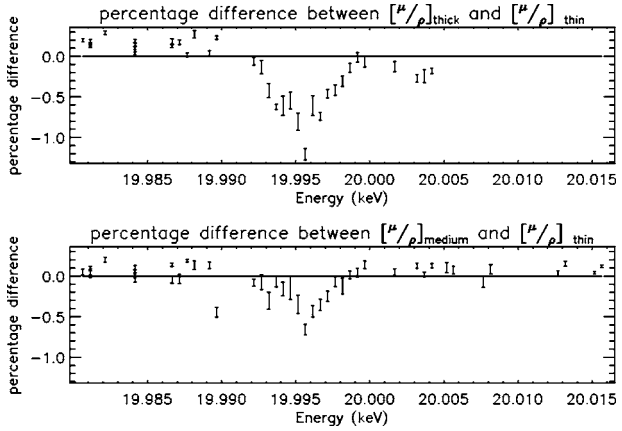

Fig. 7 Percentage difference between the mass attenuation coefficients obtained using the thick (top) and medium (bottom) foils, and that obtained using the thin foil. The prominent dip in the discrepancies occurring at about 19.995 keV coincides with the point where the gradient of the mass attenuation coefficient reaches its maximum value (Fig. 6). A second dip, expected to occur at about 20.006 keV, is not so prominent due to the presentation of the percentage difference.

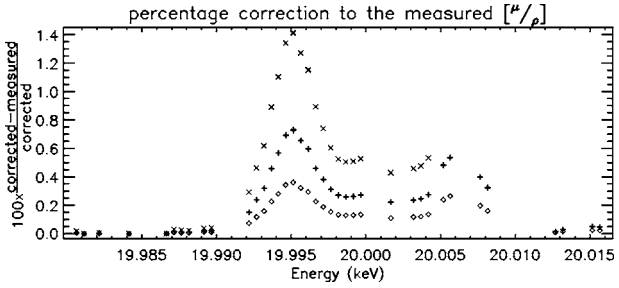

Fig. 8 Percentage correction to the mass attenuation coefficients measured in the neighborhood of the absorption edge and in the region of the XAFS, evaluated using the linearized approximation.

at the Advanced Photon Source (APS). The beam was produced by an undulator and was monochromated by reflection from the (3,1,1) planes of a pair of silicon crystals.

The values presented in Fig. 6 are in good agreement and could be used to report x-ray absorption near-edge structure (XANES), for example. However, the discrepancies between the values obtained using foils of different thickness, which cannot easily be resolved in Fig. 6, are presented in Fig. 7. This figure presents the percentage difference between the mass attenuation coefficients determined using the thick (top figure) and medium (bottom figure) foils and that determined using the thinnest foil. There is a gradient-correlated discrepancy between the measured values; the magnitude of the discrepancy increases as the thickness of the foil used to make the measurement increases.

The measured mass attenuation coefficient (subscript m) is related to the beam energy profile and the "true" mass attenuation coefficient (subscript t) by[25]

$$\exp\left(-\left[\frac{\mu}{\rho}\right]_{m,E_0}[\rho t]\right)=\int_0^\infty \tilde{I}_{E_0}\exp\left(-\left[\frac{\mu}{\rho}\right]_{t,E}[\rho t]\right)dE, \quad (3)$$

where E_0 is the central energy of the beam profile and $\tilde{I}_0$ is the normalized incident beam energy profile, defined as

$$\tilde{I}_0=\frac{I_0}{\int_0^\infty I_0 dE}. \quad (4)$$

Elsewhere, we have inverted Eq. (3) under the assumption of the approximate linearity of the mass attenuation coefficient on the scale of the beam bandwidth, and have determined the bandwidth of our x-ray beam to be 1.57 eV±0.03 eV at 20 keV.[25] We have also used the linearized approach to determine a correction to the mass attenuation coefficients measured on the absorption edge of molybdenum.[14] Figure 8 presents the correction to the mass attenuation coefficients obtained along the absorption edge, and shows that the finite x-ray bandwidth has affected the measurements by up to 1.4%. The structure shown in Fig. 8 is significant, and would be of interest to x-ray absorption fine structure (XAFS) and XANES investigations.

5 Full-Foil Mapping Technique

In a number of recent reports[17–19,26–29] it has been observed that, at between 0.5 to 2%, the dominant and limiting source of error in the measurement of mass attenuation coefficients is the accurate determination of the thickness of the absorber along the path traversed by the x-ray beam. We have developed a full-foil mapping technique for determining the mass attenuation coefficient on an absolute scale, which overcomes previous limitations due to uncertainties in the thickness of the absorber.

Traditionally, the local value of the integrated column density has been determined as the product of the density and the thickness. The local thickness was determined by a variety of techniques using micrometry,[11,12,29,20,30] profilometry,[11], optical microscopy,[31] step profilometry,[32] and x-ray scanning techniques.[11,12,20] Measurements of sample thickness have the advantage that they probe the variation of the thickness across the surface of the foil. However, each of the techniques mentioned is subject to a range of fundamental limitations affecting its precision and accuracy, which are difficult to overcome,[11,12,33] and which represent a major limitation on the precision and accuracy of the determination of the mass attenuation coefficient.

More recent measurements have used the areal density of the absorber, which we term the integrated column density, for the determination of the mass attenuation coefficient.[11,12,17–19,26,28,34–36] However, these measurements have generally been limited to accuracies of 0.5 to 2% due to variation in the thickness, which has limited the determination of the local integrated column density of the absorbing specimen along the column traversed by the beam.

The Beer-Lambert equation describes the attenuation of x-rays of a given energy passing through an absorber by

$$-\ln\left(\frac{I}{I_0}\right)_{xy}=\left[\frac{\mu}{\rho}\right][\rho t]_{xy}, \quad (5)$$

where I and I_0 represent the attenuated and unattenuated beam intensities, respectively, $[\mu/\rho]$ represents the mass attenuation coefficient of the absorbing material at a given energy, and $[\rho t]_{xy}$ the integrated column density along the

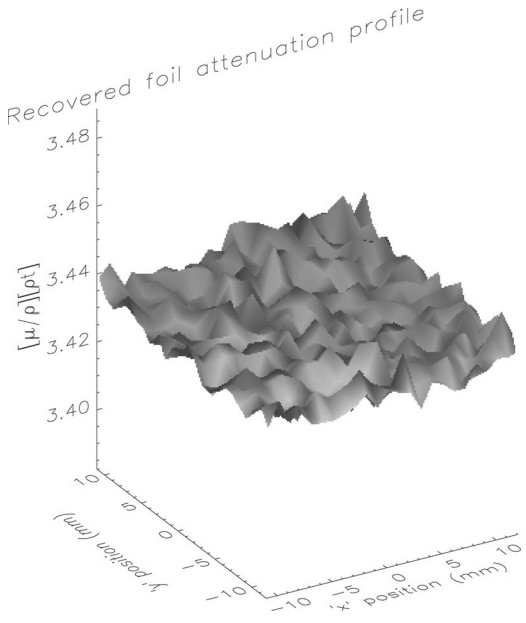

Fig. 9 Attenuation profile of a molybdenum foil. The attenuation profile was produced from an x-ray scan of the foil mounted in a plastic holder. The small holder contribution was fitted and subtracted from these measurements. The x-ray beam used to make the measurements was 1×1 mm^2 and measurements were taken at 1-mm intervals across the foil.

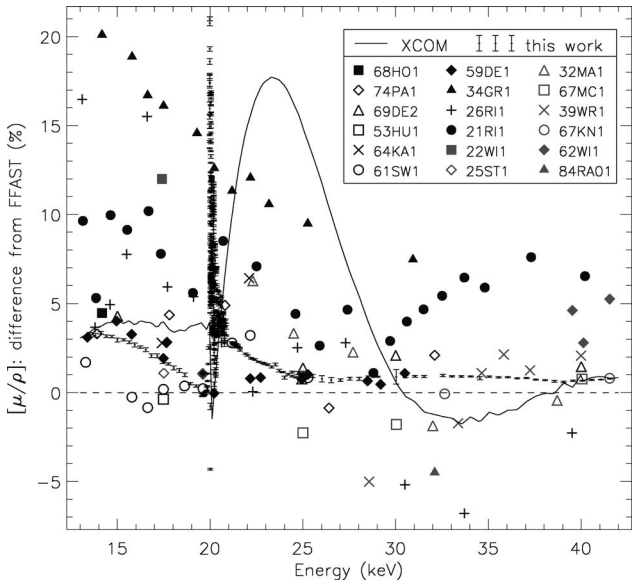

Fig. 10 Our measured values of the mass attenuation coefficients of molybdenum as a percentage difference from the tabulated FFAST values.[1–3] Measurement uncertainties of 0.02 to 0.15% are indicated by the error bars. Also shown are the percentage differences between the tabulated XCOM[4,5] values and the experimental values tabulated by Hubbell et al.,[6,7] compared with FFAST.

path taken by the x-ray beam through the location (x,y) on the absorber. It is obvious from Eq. (5) that measurements made at a single (x,y) location on an absorber cannot be used to determine the mass attenuation coefficient to a higher level of accuracy than that to which the integrated column density of the absorber at that point is known.

The mass attenuation coefficient of a foil absorber can be determined by measuring the attenuation at (x,y) locations to determine an *attenuation profile* $-\ln(I/I_0)_{xy}$ of the absorber. The mass attenuation coefficient can then be determined from the average of the measured attenuation profile, since for a homogeneous sample with fixed $[\mu/\rho]$,[37]

$$-\overline{\ln\left(\frac{I}{I_0}\right)_{xy}}=\overline{\left[\frac{\mu}{\rho}\right][\rho t]_{xy}}=\overline{\left[\frac{\mu}{\rho}\right]}\,\overline{[\rho t]_{xy}}=\left[\frac{\mu}{\rho}\right]\frac{m}{A}, \tag{6}$$

where the mass m of a given area A of the foil is used to determine the average integrated column density $\overline{[\rho t]}$. The mass and area of the foil can be measured to high accuracy using well-established techniques, for example by using an optical comparator to determine area and an accurate microgram balance to measure mass. In sharp contrast to the previously mentioned techniques, this technique can be used to determine the mass attenuation coefficient to high accuracy without directly determining the local integrated column density at any point of the absorber.

Figure 9 shows the attenuation profile of a nominally 254-μm-thick molybdenum foil. This attenuation profile has been determined from the attenuation measurements of the sample mounted in a plastic holder. To determine the attenuation profile of the absorbing sample alone, we have subtracted the small fitted holder component from the measured attenuation profile.

Using this technique, we have recently determined the mass attenuation coefficients of molybdenum to an accuracy of 0.028%[37] and of silver to accuracies in the range 0.27 to 0.7%.[33] Measurements of the attenuation profile of the silver foils at different energies have confirmed the reproducibility of the measurement at this high accuracy.

6 Discussion: Informing Form-Factor Calculations

We have measured the mass attenuation coefficients of copper,[11] silicon,[12] silver,[13] and molybdenum[14] using various synchrotron sources. Following the principles of the XERT, measurements were made over an extended range of every dimension of the measurement parameter space, and were investigated for evidence of systematic errors. We have developed a technique to determine an accurate value of the mass attenuation coefficient from raster measurements made across the surface of an absorber. We have also detected and corrected effects resulting from a small fraction of harmonic energy components in the synchrotron beam, from fluorescent radiation produced in an absorbing specimen, and from the finite bandwidth of the x-ray beam. By applying these techniques, we have improved measurement accuracies by over an order of magnitude.

Figure 10 presents our measured values for molybdenum compared with the FFAST tabulated values. Also shown are the XCOM calculated values and the experimental values tabulated in Hubbell et al.,[6,7] compared to the FFAST values. The trend of the percentage difference between our values and the FFAST tabulation is generally smooth to within the claimed measurement uncertainty, indicating that the uncertainties are appropriately estimated. By contrast, the point-to-point variations in the trend of the measurements tabulated by Hubbell et al. are typically no better

than 1 to 2% and are therefore the limiting possible precision of any of these measurements, with the accuracy necessarily being poorer. The large inconsistencies between the different sets of measurements prove the magnitude of present systematic errors in those datasets. We believe that our measurements are free from such systematic errors because we have explicitly investigated our measurements for their presence and have proven that each has a small or negligible remaining signature in our results.

The XCOM tabulated values exhibit a large oscillation with respect to the FFAST values over the energy range from 20 keV to 30 or 40 keV. Oscillatory behavior in the calculated values has been observed elsewhere[1,2] and may be the result of an incompletely converged calculation. Our measurements clearly suggest that the XCOM tabulation is in error in this region. Above about 40 keV, the XCOM values are in good agreement with our measurements.

The FFAST tabulation estimates uncertainties—arising from calculational convergence precision and the limitations of various approximations—at about 50% within $E_K \lesssim E \lesssim 1.001E_K$, 10 to 20% within $1.001E_K \lesssim E \lesssim 1.1E_K$, 3% within $1.1E_K \lesssim E \lesssim 1.2E_K$, and 1% for $E \gtrsim 1.2E_K$ (E_K is the K-shell absorption-edge energy). These estimates are in accord with the differences of Fig. 10. The difference between our measurements and the FFAST tabulation is stable at about 0.5 to 1% at energies above 25 keV. Below the absorption edge, the measurements exhibit a more complex pattern of discrepancy, but fall between the XCOM and FFAST values.

The measured values are 1 to 3% higher than the FFAST tabulated values within a range of about 5 keV above the absorption edge. Although this is within the FFAST uncertainty, a similar above-edge enhancement observed for copper[11] and silver[13] suggests that the FFAST values are systematically low in this region. The presence of this discrepancy in measurements of three elements indicates new physics in the above-edge energy region.[13,14,38,39] Further experiments are required to determine whether this discrepancy is present for other elements and above other (e.g., L-shell) absorption edges. Such measurements will provide further clues that will inform future calculations of the mass attenuation coefficients.

Acknowledgments

We acknowledge the assistance of the synchrotron staff at each of the beamline facilities involved in this work, being beamline 20B of the Photon Factory in Tsukuba, and beamlines 1-BM, 1-ID, and 12-BM of the APS. This work was supported by the Australian Synchrotron Research Program, which is funded by the Commonwealth of Australia under the Major National Research Facilities Program, and by a number of grants of the Australian Research Council. Use of the Advanced Photon Source was supported by the U.S. Department of Energy, Basic Energy Sciences, Office of Energy Research, under contract number W-31-109-Eng-38. Author de Jonge acknowledges the Australian Optical Society and SPIE for their support and thanks them for a scholarship that enabled him to present this work.

References

1. C. T. Chantler, "Detailed tabulation of atomic form factors, photoelectric absorption and scattering cross section, and mass attenuation coefficients in the vicinity of absorption edges in the soft x-ray (Z=30–36, Z=60–89, E=0.1 keV–10 keV), addressing convergence issues of earlier work," *J. Phys. Chem. Ref. Data* **29**, 597–1056 (2000).
2. C. T. Chantler, "Theoretical form factor, attenuation and scattering tabulation for Z=1–92 from E=1–10 eV to E=0.4–1.0 MeV," *J. Phys. Chem. Ref. Data* **24**, 71–85 (1995).
3. C. T. Chantler, K. Olsen, R. A. Dragoset, A. R. Kishore, S. A. Kotochigova, and D. S. Zucker, "*X-Ray form factor, attenuation and scattering tables (version 2.0)*," See http://physics.nist.gov/ffast, National Institute of Standards and Technology, Gaithersburg, MD (2003).
4. M. J. Berger, J. H. Hubbell, S. M. Seltzer, J. S. Coursey, and D. S. Zucker, "*XCOM: photon cross section database (version 1.2)*," See http://physics.nist.gov/xcom, National Institute of Standards and Technology, Gaithersburg, MD (1999).
5. M. J. Berger and J. H. Hubbell, "Photon cross sections on a personal computer," *Natl. Stand. Ref. Data Ser.* **87**, 3597 (2004); http://physics.nist.gov/xcom.
6. J. H. Hubbell, "*NISTIR 5437*," National Institute of Standards and Technology, Gaithersburg, MD (1994).
7. J. H. Hubbell, J. S. Coursey, J. Hwang, and D. S. Zucker, "*Bibliography of photon total cross section (attenuation coefficient) measurements (version 2.3)*," See http://physics.nist.gov/photoncs, National Institute of Standards and Technology, Gaithersburg, MD (2003).
8. D. C. Creagh and J. H. Hubbell, "Problems associated with the measurement of x-ray attenuation coefficients. I. Silicon. Report on the International Union of Crystallography X-ray Attenuation Project," *Acta Crystallogr.* **43**, 102–112 (1987).
9. D. C. Creagh and J. H. Hubbell, "Problems associated with the measurement of x-ray attenuation coefficients. II. Carbon. Report on the International Union of Crystallography X-ray Attenuation Project," *Acta Crystallogr.* **46**, 402–408 (1990).
10. C. T. Chantler, C. Q. Tran, D. Paterson, D. Cookson, and Z. Barnea, "X-ray extended-range technique for precision measurement of the x-ray mass attenuation coefficient and Im(f) for copper using synchrotron radiation," *Phys. Lett. A* **286**, 338–346 (2001).
11. C. T. Chantler, C. Q. Tran, Z. Barnea, D. Paterson, D. J. Cookson, and D. X. Balaic, "Measurement of the x-ray mass attenuation coefficient of copper using 8.85–20 keV synchrotron radiation," *Phys. Rev. A* **64**, 062506 (2001).
12. C. Q. Tran, C. T. Chantler, Z. Barnea, D. Paterson, and D. J. Cookson, "Measurement of the x-ray mass attenuation coefficient and the imaginary part of the form factor of silicon using synchrotron radiation," *Phys. Rev. A* **67**, 042716 (2003).
13. C. Q. Tran, C. T. Chantler, Z. Barnea, M. D. de Jonge, B. B. Dhal, C. T. Y. Chung, D. Paterson, and J. Wang, "Measurement of the x-ray mass attenuation coefficient of silver using the x-ray-extended range technique," *J. Phys. B* **38**(1), 89–107 (2005).
14. M. D. de Jonge, C. Q. Tran, C. T. Chantler, Z. Barnea, B. B. Dhal, D. J. Cookson, W.-K. Lee, and A. Mashayekhi, "Measurement of the x-ray mass attenuation coefficient and determination of the imaginary component of the atomic form factor of molybdenum over the 13.5–41.5-keV energy range," *Phys. Rev. A* **71**(3), 032702 (2005).
15. J. H. Beaumont and M. Hart, "Multiple Bragg reflection monochromators for synchrotron x-radiation," *J. Phys. E* **7**, 823–829 (1974).
16. U. Bonse, G. Materlik, and W. J. Schröder, "Perfect-crystal monochromators for synchrotron x-radiation," *J. Appl. Crystallogr.* **9**, 223–230 (1976).
17. R. Nathuram, I. S. S. Rao, and M. K. Mehta, "Photoelectric cross sections for 6–20-keV photons in beryllium, carbon, magnesium, aluminum, silicon, copper, silver, and lead," *Phys. Rev. A* **37**, 4978–4981 (1988).
18. F. Machali, G. G. Al-Barakati, A. A. El-Sayed, and W. J. Altaf, "The photoelectric cross section of gamma rays in the energy range 43 to 152 keV," *J. Phys. F: Met. Phys.* **17**, 1279–1284 (1987).
19. L. Gerward, "X-ray attenuation coefficients of carbon in the energy range 5 to 20 keV," *Acta Crystallogr.* **39**, 322–325 (1983).
20. J. F. Mika, L. J. Martin, and Z. Barnea, "X-ray attenuation of silicon in the energy range 25–50 keV," *J. Phys. C* **18**, 5215–5223 (1985).
21. C. T. Chantler, C. Q. Tran, D. Paterson, Z. Barnea, and D. J. Cookson, "Monitoring fluctuations at a synchrotron beamline using matched ion chambers. I. Modelling, data collection and deduction of simple measures of association," *X-Ray Spectrom.* **29**(6), 449–458 (2000).
22. C. T. Chantler, C. Q. Tran, D. Paterson, D. J. Cookson, and Z. Barnea, "Monitoring fluctuations at a synchrotron beamline using matched ion chambers. II. Isolation of component noise sources, and application to attenuation measurements showing increased precision by two orders of magnitude," *X-Ray Spectrom.* **29**(6), 459–466 (2000).
23. C. Q. Tran, Z. Barnea, M. D. de Jonge, B. B. Dhal, D. Paterson, D. J. Cookson, and C. T. Chantler, "Quantitative determination of major systematics in synchrotron x-ray experiments: seeing through har-

monic components," *X-Ray Spectrom.* **32**, 69–74 (2003).
24. C. Q. Tran, M. D. de Jonge, Z. Barnea, and C. T. Chantler, "Absolute determination of the effect of scattering and fluorescence on x-ray attenuation measurements," *J. Phys. B* **37**, 3163–3176 (2004).
25. M. D. de Jonge, Z. Barnea, C. Q. Tran, and C. T. Chantler, "X-ray bandwidth: determination by on-edge absorption and effect on various absorption experiments," *Phys. Rev. A* **69**, 022717 (2004).
26. W. Dachun, D. Xunliang, W. Xinfu, Y. Hua, Z. Hongyu, S. Xinyin, and Z. Guanghua, "X-ray attenuation coefficients and photoelectric cross sections of Cu and Fe in the range 3 keV to 29 keV," *Nucl. Instrum. Methods Phys. Res. B* **71**, 241–248 (1992).
27. D. K. S. Reddy, K. Premachand, V. R. K. Murty, J. R. Rao, and V. Lakshminarayana, "Photoelectric interaction below the *K* edge," *Phys. Rev. A* **13**, 326–329 (1976).
28. L. Unonius and P. Suortti, "Mass attenuation coefficients of the elements Ti, V, Fe, Co, Ni, Cu and Zn for the *K*-emission lines between 4.51 and 10.98 keV," *J. Appl. Crystallogr.* **22**, 46–52 (1989).
29. L. Gerward, "X-ray attenuation coefficients and atomic photoelectric absorption cross sections of silicon," *J. Phys. B* **14**, 3389–3395 (1981).
30. A. A. Berry and J. L. Lawrence, "X-ray attenuation coefficients of graphite in the range 0.40 to 1.54 Å," *Acta Crystallogr.* **35**, 316–318 (1979).
31. J. Balthazar-Rodrigues and C. Cusatis, "Determination of x-ray photoelectric absorption of Ge and Si avoiding solid-state effects," *Nucl. Instrum. Methods Phys. Res. B* **179**, 325–333 (2001).
32. Z. H. Levine, S. Grantham, and I. McNulty, "Mass absorption coefficient of tungsten for 1600–2100 eV," *Phys. Rev. B* **65**, 064111 (2002).
33. C. Q. Tran, Z. Barnea, C. T. Chantler, and M. D. de Jonge, "Accurate determination of the thickness or mass per unit area of thin foils and single-crystal wafers for x-ray attenuation measurements," *Rev. Sci. Instrum.* **75**(9), 2943–2949 (2004).
34. M. Angelone, T. Bubba, and A. Esposito, "Measurement of the mass attenuation coefficient for elemental materials in the range $6 \leqslant Z \leqslant 82$ using x-rays from 13 up to 50 keV," *Appl. Radiat. Isot.* **55**(4), 505–511 (2001).
35. L. Gerward, "X-ray attenuation coefficients of beryllium in the energy range 5 to 20 keV," *Acta Crystallogr.* **45**, 1–3 (1989).
36. R. S. Prakhya, K. Parthasaradhi, V. Lakshminarayana, K. L. Narasimham, K. V. Ramanaiah, and S. B. Reddy, "Measurement of *K*-shell photoelectric cross sections by the indirect method," *Phys. Rev. A* **33**, 2440–2443 (1986).
37. M. D. de Jonge, Z. Barnea, C. T. Chantler, and C. Q. Tran, "Full-foil x-ray mapping of integrated column density applied to the absolute determination of mass attenuation coefficients," *Meas. Sci. Technol.* **15**, 1811–1822 (2004).
38. D. C. Creagh, "The use of the form factor formalism in crystallography," *Nucl. Instrum. Methods Phys. Res. A* **280**, 180–188 (1989).
39. D. C. Creagh, "The atomic form factor, the dispersion corrections and their role in x-ray crystallography," *Chin. J. Phys. (Taipei)* **29**(4), 299–325 (1991).

Martin de Jonge has recently completed a doctoral thesis, wherein he developed methods for making accurate measurements of the imaginary component of the atomic form-factor, Im(f). His measurements of molybdenum are the most accurate of their type, sufficient to challenge fundamental atomic theory. In 2002 he was awarded an OSA / SPIE travel prize, which enabled him to travel to the United States to present this research, and which ultimately resulted in this work. He is currently enjoying a postdoctoral position at the intermediate-energy 1 to 4 keV beamline at the APS, where he is developing techniques of coherent diffraction imaging.

Chanh Q. Tran obtained his PhD in 2002 on the development of the x-ray extended-range technique, which enables precision calibration of synchrotron beamline optics and sets the current standard for experimental determination of x-ray photon-atom interactions. Despite being in an early stage of his research career, he has already published 23 refereed papers including those in Physical Review Letters and Physical Letters. His other research covers a broad range of activities including x-ray coherence, imaging, and interference.

Chris Chantler is an associate professor and reader at the School of Physics, University of Melbourne. He obtained his DPhil from Oxford in 1990, is a Councillor of the Australian Optical Society, and associate editor of *AOS News*; scientific program chair of X-ray and Inner-Shell Processes 2005, and guest editor of the refereed *Proceedings in Radiation Physics and Chemistry*; a member of the Optical Society of America and the American Institute of Physics since 1993; and a member of the Australian Institute of Physics since 1992. He has made seminal developments in the computation of x-ray atomic form-factor theory, and his theory is the current NIST reference database on the subject. The Web database has received 1200 or more hits per month since its electronic installation as one of the three major references for atomic form factors and attenuation coefficients. He has formulated the first dynamical theory of curved nonideally imperfect crystal x-ray diffraction, essential for accurate interpretation of such experiments. He has built and directed the x-ray facility at the University of Melbourne over the last ten years since returning to Australia from the United States. He has 72 papers submitted or published in refereed journals and more than 180 papers and conference presentations, with over 94 citations on an individual publication.

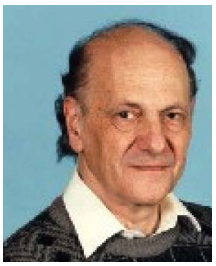

Zwi Barnea is an associate and associate professor emeritus of the School of Physics, University of Melbourne. He obtained his doctorate there in 1974. He is among the few world leaders who have claimed and delivered 1% accuracy in form-factor experiments. He has more than 52 publications in the field. His main contributions have been in developing new methods of x-ray intensity measurements and applying these to accurate measurements of structure factors, temperature factors, anharmonic thermal motion, bonding electron redistribution, anomalous dispersion effects, Bijvoet ratios, absolute intensity measurements of Bragg reflections, and determination of extinction effects in real crystals. He contributed to the design of "Big Diff," a multipurpose instrument on Australia's synchrotron beamline in Tsukuba. This is a major success of Australian synchrotron development, and has been used in various collaborations for measurements of x-ray absorption, phase retrieval, and diffuse scattering by metallic multilayers. He also developed methods for producing x-ray capillary optics for synchrotron beamlines and rotating anode laboratory generators, where the use of capillaries made it possible for the first time to study (30-μm) microcrystals of proteins in the laboratory.